Improved Damage-Tolerance Analysis Methodology

J B Chang *
Rockwell International, Los Angeles, California
and
R M Engle †
Wright-Patterson Air Force Base, Dayton, Ohio

A computerized damage tolerance analysis methodology, which can be reliably used to predict the fatigue crack growth behavior and lives of various types of cracks contained in metallic structures, subjected to complex spectrum loadings, has been developed This analysis method was developed primarily for the performance of the damage-tolerance analysis in the detail design stage of any aircraft system A state of the art load interaction model, which accounts for both retardation and acceleration, as well as their coupling effect to crack growth behavior, has been incorporated in this analysis methodology in order to predict fatigue crack lives more ac curately A two dimensional growth option is provided to account for the shape change effect of part through cracks (PTC) such as surface flaws and corner cracks at holes. A linear approximation technique is used as the damage accumulation scheme for saving computation costs This methodology has been implemented into a new computer code, the CRKGRO program A series of crack growth data correlation studies has been conducted using CRKGRO Results demonstrated that this damage tolerance analysis methodology provides reliable predictions on fatigue crack growth lives for cracked specimens subjected to spectrum loadings of various classes of aircraft

Introduction

THE Air Force damage tolerance requirements levied on military aircraft,[1,2] and the new damage-tolerance requirements applied to the commercial transports,[3] have necessitated the development of analytical methods and automated crack growth analysis computer codes These codes predict the fatigue growth behavior and lives of cracks or cracklike flaws contained in primary airframe structures under complex flight spectrum loadings Many computer codes have been developed in the last decade to perform such tasks These include CRACKS[4] developed by the Air Force, the EFFGRO program[5] developed at Rockwell originally for the B 1 strategic bomber, the FLAGRO program[6] developed at Rockwell for the Space Shuttle, the CRG GD program[7] used for damage tolerance evaluation of the F 16, and the FAST program,[8] just to name a few. However, the crack growth methodologies incorporated in most of these com puter codes have drawbacks. A majority of the codes do not account for shape change effects on growth behavior of the part-through crack (PTC) including surface flaws, corner cracks at fastener holes or cutouts, etc , thus introducing errors in the predictions of critical crack sizes and lives for shallow or deep cracks contained in structures under axial tension or bending loadings [9,10] A few programs do not account for the tensile overload retardation effect. This results in conservative predictions for spectrum loads consisting of many overload cycles [11] Many programs do not account for the compressive load acceleration effects and end up overestimating the lives for cracks contained in structures subjected to cyclic loadings consisting of large amounts of tension compression cycles [11-13] Some programs use numerical integration techniques such as the Runge Kutta method[14] to perform damage accumulation calculations For spectrum loading cases, computation costs to run those programs are very high; therefore, they are not cost-effective

Recently, a new computer code, the CRKGRO program,[15] has been developed by Chang et al at Rockwell under an Air Force-sponsored project [16] CRKGRO was developed to perform detailed fatigue crack growth analysis on a cycle-by cycle basis The fatigue crack growth prediction method incorporated in this computer code is an improved methodology that overcomes most of the aforementioned drawbacks A correlation study has been conducted to assess the prediction accuracy of the CRKGRO program using crack growth test data generated under typical fighter, bomber, and transport spectra This paper describes the technical details of the damage tolerance analysis methodology incorporated in CRKGRO. The results of the correlation study are also presented

Fatigue Crack Growth Prediction Methodology

The crack growth analysis methodology incorporated in CRKGRO is based on the linear elastic fracture mechanics (LEFM) concept; that is, the range of the crack tip stress intensity factor, Δk, is the controlling parameter for characterizing the growth rate of a crack under cyclic loadings. For the performance of a detail fatigue crack growth analysis, the following elements are interrelated: 1) a fatigue crack growth rate model and the corresponding growth rate constants; 2) a load interaction model which accounts for retardation and acceleration effects to the crack growth; 3) a description of the stress spectrum; 4) initial crack types, sizes, and dimensions of the structure which contains the crack; 5) crack tip stress intensity factor solutions; and 6) a damage accumulation procedure

Fatigue Crack Growth Rate Models

For constant amplitude loadings, the baseline fatigue crack growth rate models used in this program are the modified Walker equation[17] for positive stress ratios and the Chang equation[16] for negative stress ratios. In mathematical forms,

Presented as Paper 83-0863 at the AIAA/ASME/ASCE/AHS 24th Structures Structural Dynamics and Materials Conference Lake Tahoe, Nev , May 2 4 1983; received Aug 8 1983; revision received March 26, 1984

*North American Aircraft Operations; presently Engineering Specialist The Aerospace Corporation Los Angeles California
†Aerospace Engineer

they can be expressed as follows:

For $\Delta K > \Delta K_{th}$ $R \geq 0$

$$da/dN = C[\Delta K/(1-\bar{R})^{1-m}]^n$$

$$\bar{R} < R^+_{cut}\ \bar{R} = R$$

$$\bar{R} > R^+_{cut}\ \bar{R} = R^+_{cut}$$

For $\Delta K > \Delta K_{th}$ $R < 0$

$$da/dN = C[(1+\bar{R}^2)^q K_{max}]^n$$

$$\bar{R} \geq R^-_{cut}\ \bar{R} = R$$

$$\bar{R} < R^-_{cut}\ \bar{R} = R^-_{cut}$$

For $\Delta K \leq \Delta K_{th}$

$$da/dN = 0$$

where C and n are the growth rate constants, R the stress ratio, ΔK the range of the stress intensity factor, m the stress ratio collapsing factor, q the negative R effect factor and R^+_{cut} the cutoff values for the stress ratios either positive or negative

The threshold stress intensity factor range ΔK_{th} is deter mined by

$$\Delta K_{th} = (1-AR)\Delta K_{th_o}$$

where ΔK_{th_o} is the threshold value of the stress intensity factor range obtained from $R=0$ constant amplitude tests; A an empirical constant determined from constant-amplitude test data with various stress ratios The procedure for determining crack growth rate constants is discussed in Ref 15

Load Interaction Model

To account for the retardation effect, the generalized Willenborg model[18] is adopted in CRKGRO The generalized Willenborg model can be written in the following form:

$$(K_{max})_{eff} = K_{\infty_{max}} - \phi\left[K^{oL}_{max}\left(1-\frac{\Delta a}{Z_{oL}}\right)^{1/2} - K_{\infty_{max}}\right]$$

$$(K_{min})_{eff} = K_{\infty_{min}} - \phi\left[K^{oL}_{max}\left(1-\frac{\Delta a}{Z_{oL}}\right)^{1/2} - K_{\infty_{max}}\right]$$

and

$$\phi = \left[1-(K_{maxTH}/K_{max})/(R_{SO}-1)\right]$$

where $K_{\infty_{max}}$ is the stress intensity factor corresponding to the maximum remotely applied stress, K^{oL}_{max} is the stress intensity factor corresponding to the maximum stress of the overload, Δa is the incremental growth following the overload, and Z_{oL} is the overload interaction zone size R_{SO} is the overload shutoff ratio which is defined as:

$$R_{SO} = K^{oL}_{max}/K_{\infty_{max}}$$

For spectrum loading, the effective stress intensity factor range and effective stress ratio, which are used in CRKGRO, are expressed in terms of the maximum effective stress in tensity factors as follows:

$$\Delta K_{eff} = (K_{max})_{eff} - (K_{min})_{eff}$$

$$R_{eff} = (K_{min})_{eff}/(K_{max})_{eff}$$

In the load interaction accounted for option CRKGRO uses the following equation to account for tensile overload retardation effect:

For $\Delta K_{eff} > \Delta K_{th}$ $R_{eff} \geq 0$

$$da/dN = C\left[(\Delta K)_{eff}/(1-\bar{R}_{eff})1-m\right]^n$$

$$\bar{R}_{eff} \leq R^+_{cut}, \bar{R}_{eff} = R_{eff}$$

$$\bar{R}_{eff} < R^+_{cut}, \bar{R}_{eff} = R^+_{cut}$$

For $\Delta K_{th} \leq \Delta K_{th}$

$$da/dN = 0$$

where C n m and R^+_{cut} are the same crack growth rate parameters described under "Fatigue Crack Growth Rate Models." The threshold values of the stress intensity factor range are also identical to those used in the constant amplitude cases

If the effective stress ratio is negative (i e $R_{eff} < 0$), the Chang negative stress ratio equation is used, which accounts for the compressive load acceleration effect:

$$da/dN = C\left[(1+R^{-2}_{eff})^q (K_{max})_{eff}\right]^n$$

$$\bar{R}_{eff} \geq \bar{R}_{cut}, \bar{R}_{eff} = R_{eff}$$

$$\bar{R}_{eff} < \bar{R}_{cut}\ \bar{R}_{eff} = \bar{R}_{cut}$$

where q is the negative R ratio factor determined from test data generated for a specific negative stress ratio ($R<0$) and its $R=0$ counterpart

The reduction of the overload retardation effect caused by a compressive spike load immediately following the tensile overload, is accounted for by CRKGRO through an effective overload interaction zone concept proposed by Chang et al.[13] The effective overload interactive zone is defined in terms of the negative effective stress ratio ($R_{eff} < 0$) as:

$$(Z_{ol})_{eff} = (1+R_{eff})(Z_{ol})$$

$$\bar{R}_{eff} \geq \bar{R}_{cut}\ \bar{R}_{eff} = R_{eff}$$

$$\bar{R}_{eff} < \bar{R}_{cut}\ \bar{R}_{eff} = \bar{R}_{cut}$$

where Z_{oL} is the plastic zone size introduced by the tensile overload

In CRKGRO, the plane strain plastic zone size is used if the stress intensity factor at the maximum depth for a part through crack is to be calculated The plane stress plastic zone size is used at the length direction for through cracks and part through cracks The plane stress and plane strain plastic zone sizes are:

$$(Z_{oL})_{plane\ strain} = \frac{1}{6\pi}\left(\frac{K_{\infty_{max}}}{F_{ty}}\right)^2$$

$$(Z_{oL})_{plan\ stress} = \frac{1}{2\pi}\left(\frac{K_{\infty_{max}}}{F_{ty}}\right)^2$$

where F_{ty} is the material tensile yield strength

Two Dimensional Crack Growth Analysis

For PTCs, CRKGRO accounts for the shape change effects through the two dimensional (2 D) crack growth analysis

approach The 2 D crack growth analysis approach assumes that growth in the two principal directions of a PTC can be characterized by the stress intensity factors at the extreme points of each direction In constant amplitude loadings for example, the crack growth rates at the two extreme points (A and B of a surface crack as shown in Fig 1) are calculated by CRKGRO using the following set of equations:

$$da/dN = C_A\left[\Delta K_A/(1-R)^{1-m_A}\right]^{n_A}$$
$$da/dN = C_B\left[\Delta K_B/(1-R)^{1-m_B}\right]^{n_B}$$

where C_A n_A, m_A and C_B n_B m_B are the material's crack growth rate parameters along the depth and length directions, respectively; R is the cyclic stress ratio; and ΔK_A and ΔK_B are the stress-intensity factor range at the maximum depth and length points, respectively

Stress intensity factors at maximum depth point A and maximum length point B built into CRKGRO are prepared using the compound solution format In general, these can be expressed as:

$$K_A = \left[F_A\left(\frac{a}{t}\ \frac{a}{c}\ \frac{c}{b}\right)\right]\sigma\sqrt{\frac{a}{Q}} \quad \text{at the maximum depth}$$
$$K_B = \left[F_B\left(\frac{a}{t}\ \frac{a}{c}\ \frac{c}{b}\right)\right]\sigma\sqrt{\frac{c}{Q}} \quad \text{at the maximum length}$$

where a is the depth c the half length for a surface crack, t the thickness of the structure b the half width of the structure, Q the shape factor and F_A and F_B the geometrical magnification factors for the maximum depth point A and the maximum length point B as shown in Fig 1

In CRKGRO, the geometrical magnification factors are in a polynomial format For the surface crack shown in Fig 1, the geometrical magnification factors are derived from the general surface crack stress intensity factor solution proposed by Newman and Raju [19] At point B, the solution was derived from $\phi = 10$ deg due to the boundary-layer effect near the intersection of the crack with a free surface [20]

At point A ($\phi = 90$ deg),

$$F_A = \left\{1\ 13 - 0\ 09\ (a/c) + \left[\frac{0\ 89}{(0\ 2 + a/c)} - 0\ 54\right]\left(\frac{a}{t}\right)^2 + \left[0\ 5 - \frac{1}{(0\ 65 + a/c)} + 14(1-a/c)^{24}\right]\left(\frac{a}{t}\right)^4\right\}$$

At point B ($\phi = 10$ deg),

$$F_B = \left\{1\ 13 - 0\ 09(a/c) + \left[\frac{0\ 89}{(0\ 2 + a/c)} - 0\ 54\right]\left(\frac{a}{t}\right)^2 + \left[0\ 5 - \frac{1}{(0\ 65 + a/c)} + 14(1-a/c)^{24}\right]\left(\frac{a}{t}\right)^4\right\} \times \left\{[1\ 1 + 0\ 35(a/t)^2]\left(\frac{a}{c}\right)\sqrt{\sec\left[\left(\frac{\pi c}{2b}\right)\sqrt{\left(\frac{a}{t}\right)}\right]}\right\}$$

The shape factor Q used in CRKGRO is also in a closed form solution format, which is expressed as

$$Q = [1 + 1\ 464(a/c)^{1\ 65}]$$

Crack Tip Stress Intensity Factor Solutions

A collection of stress intensity factor solutions for various through and part-through crack configurations has been incorporated into CRKGRO through a CRACK LIBRARY module which consists of separate subroutines, each containing one stress intensity factor solution A crack code system is used in CRKGRO For example, crack code 1010 is the surface flaw and 2010 is the centered through crack. Each PTC subroutine has two sets of solutions, K_A and K_C The stress intensity factor for a shallow crack ($a/c \leq 1$) and for a deep crack ($a/c > 1$) are included in the same subroutine A total of ten stress intensity factor solutions have been incorporated in the CRACK LIBRARY module Reference 15 contains these ten sets of solutions

For part through cracks, the CRKGRO program also provides the one dimensional (1 D) crack growth analysis option. For the 1 D option, only the stress intensity factor at the maximum depth of a PTC is calculated The aspect ratio ($a/2c$) is assumed to be constant through the whole period of the growth of the PTC (i e , the shape change of a PTC is not accounted for in the crack growth analysis)

The 1 D stress intensity factor solutions for various part through cracks, such as the surface crack, the edge corner crack and a corner crack at open holes, are presented in Ref

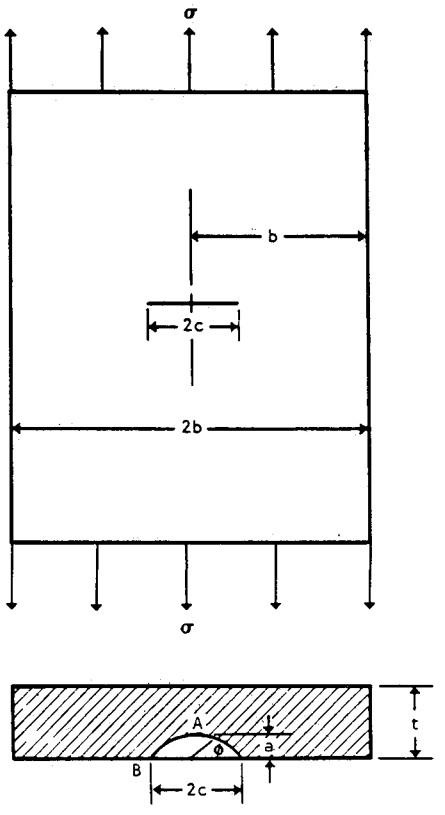

Fig 1 A typical surface crack configuration

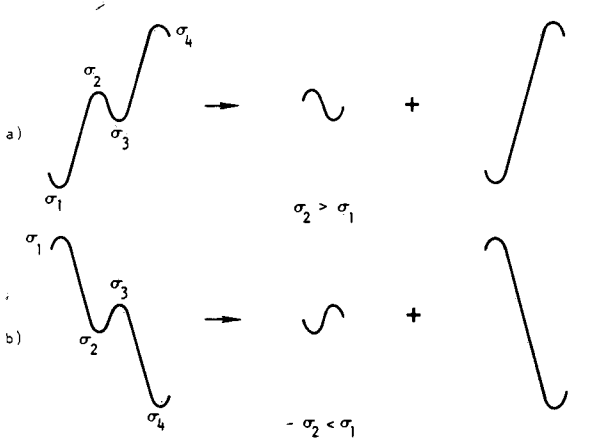

Fig 2 Range pair technique of counting spectrum load cycles

15 These solutions are different than its 2 D option coun terpart due to the fact that the shape change effect is not accounted for in the 1 D option The 1 D solutions were formulated using the compound solution technique with the average value used for the geometry correction factor

Cycle Counting Method

A cycle counting subroutine, CYCCNT, developed by Streitmatter[21] has been incorporated into CRKGRO This cycle counting subroutine uses the range-pair counting method[22] to count the cycles for spectrum loadings The essence of the range pair counting techniques can be illustrated by considering the load trace as shown in Fig 2 The criteria for counting a cycle are as follows:

1) If $\sigma_2 > \sigma_1$(Fig 2a), then a cycle of amplitude $|\sigma_2 - \sigma_3|/2$ and the mean of $|\sigma_2 + \sigma_3|/2$ is counted if $\sigma_2 \leq \sigma_4$ and $\sigma_3 \geq \sigma_1$

2) If $\sigma_2 < \sigma_1$ (Fig 2b) the same cycle is counted if $\sigma_2 \geq \sigma_4$ and $\sigma_3 \leq \sigma_1$

Starting at the beginning of a load trace, four consecutive peaks and valleys are considered If the second and third peak or valley meet the preceding conditions, one cycle is defined and those two points are deleted from the load trace The fourth peak or valley now becomes the second, and the next consecutive peak and valley of the load trace are added to again form a four-point set This counting continues until the four points being considered cannot define a cycle When this occurs, the first point will be omitted from consideration and put into a residual trace, and the next peak is added to the load trace This process continues, adding points to the residual trace as necessary, until only two or three points are left These points are added to the residual trace, which is then treated in the same manner as the original trace The results of this process leave a residual trace as shown in Fig 3 This residual trace will not be range pair counted.

Instead, these remaining cycles are to be counted such that the highest peak is paired with the lowest valley to form a cycle Moving away from this cycle in both directions each successful peak and valley are paired together If there is an extra peak or valley left on either side it will be omitted A peak on one side of the maximum excursion cycle will not be paired with a valley on the other side. Because of the load interaction effects to the crack growth behavior the sequence of the load cycles is very important Hence, the cycles are ordered based on the same order of the peaks as in the original load trace The load cycles resulting from this counting procedure will thus form the load spectrum to be used in crack growth analysis

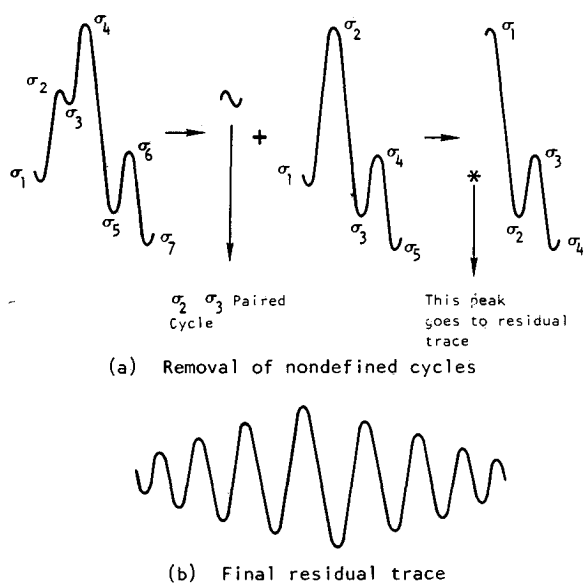

Fig 3 Range pair counting of nondefined load cycles

Damage Accumulation Technique

The Vroman linear approximation method[23] has been incorporated into this computer program as the damage accumulation scheme For a given load spectrum as shown in Table 1, the Vroman damage accumulation scheme proceeds by considering a load step (i) and using $\sigma\max_i$ and $\sigma\min_i$ to calculate $(da/dN)_i$ The value of $(0\ 01a)/dN)_i$ is then com pared to N_i where a is the instantaneous crack size If $(0\ 01a)/(da/dN)_i$ is greater than N_i, then the crack growth for that particular load step is $\Delta a = N_i \times (da/dN)_i$ The crack has then grown from a to $(a + \Delta a)$, and the program proceeds to the next load step

If $(0\ 01a)/(da/dN)_i$ is less than or equal to N_i the crack size will be $(a + 0\ 01a)$ and this load step is re examined This process continues with $(0\ 01a)/(da/dN)_i$ being compared to the remaining cycles in the step When all load steps in the block or flight have been examined the program then proceeds to the first step of the next block (or flight) and continues

Fatigue Crack Growth Data Correlations

In order to verify the previously described fatigue crack growth prediction methodology, which has been implemented into CRKGRO, a series of spectrum loading fatigue crack growth data correlation studies have been conducted Test data employed in these correlation studies were selected from various flight spectrum loading tests, which include a multimission fighter spectrum variation test a bomber spectrum test and an advanced transport airplane spectrum variation test Various types of materials and crack specimens

Table 1 Typical stress spectrum table (schematic)

Step	Maximum stress	Minimum stress	No of cycles/ block (flight)
1	σ_{max_1}	σ_{min_1}	N_1
2	σ_{max_2}	σ_{min_2}	N_2
3	σ_{max_3}	σ_{min_3}	N_3
i	σ_{max_i}	σ_{min_i}	N_i

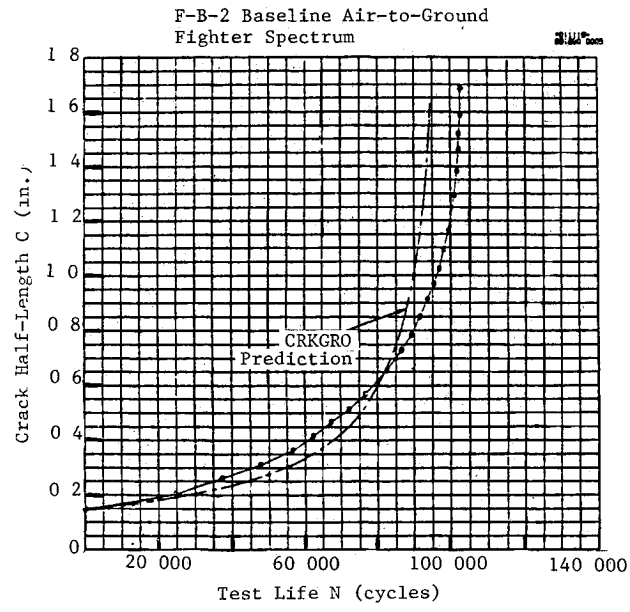

Fig 4 Crack-growth correlations—fighter air to ground baseline mission spectrum test data

were covered in these test programs The test materials were commonly used airframe materials including 2024 T851, 2219 T851 aluminum alloys HP 9Ni 4Co – 0 2C, PH 13 8 steel alloys, and 6Al 4V titanium alloy The test specimens consisted of different crack configurations such as corner cracks at fastener holes surface flaws and center through cracks

The correlation studies were performed first to conduct analytical crack growth life predictions on test cases by running CRKGRO The results of the predictions were then compared with the test data. Figure 4 shows a typical comparison of this kind plotted in the crack size (a) vs life (N) form The ratios of the predicted life (N_p) to the test life (N_t) of the correlated cases were then calculated A perfect prediction is $(N_p/N_t) = 1\ 0$ If the prediction ratio is less than 1 0 the prediction is considered to be conservative. On the contrary, the prediction is unconservative if the prediction ratio is greater than 1 0 The following paragraphs summarize the results of the fighter, bomber, and transport spectrum fatigue crack growth data correlation studies

Fighter Spectra Test Data Correlations

A total of 33 random flight spectrum loading test data[16] were correlated in this group It consisted of four baseline mission tests and 29 spectrum variation tests The four baseline missions were the air to air (A A), air to ground (A G) instrumentation navigation (I N), and composite mission of a typical fighter The spectra were in the random cycle by cycle format Each spectrum consisted of approximately 5000 nonrepeatable cycles which represented approximately 200 flights Spectrum variation parameters tested were stress levels, amount of compressive loads, high load clippings, low load truncations mission sequences, and mission mixes All test specimens were the center cracked tension (CCT) panels, machined from a single heat of 2219 T851 aluminum plates The center notches were installed through the electric discharge machining (EDM) process. Test specimens were precracked before the application of the spectrum loading All tests were conducted at room temperature in laboratory air environment

Fatigue crack growth rate constants and load interaction model parameters for the 2219 T851 aluminum alloy used in the predictions are summarized in Table 2. All random flight spectra were range pair counted before the performance of the crack growth analyses. Both the "load interaction" solutions and "without load interaction" solutions were obtained for all test cases The without load-interaction

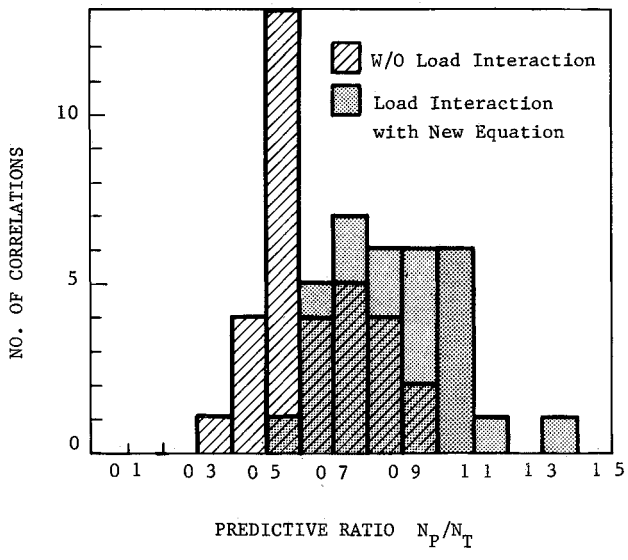

Fig 5 Histogram—CRKGRO life predictions correlated with fighter spectrum test data

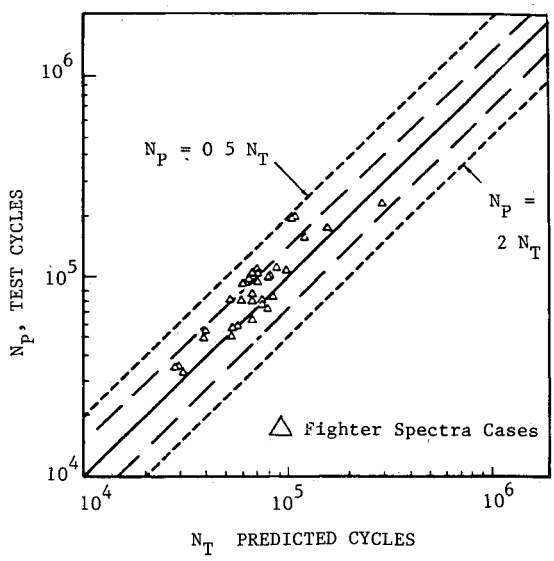

Fig 6 Correlation of fighter test results—CRKGRO with load interaction predictions

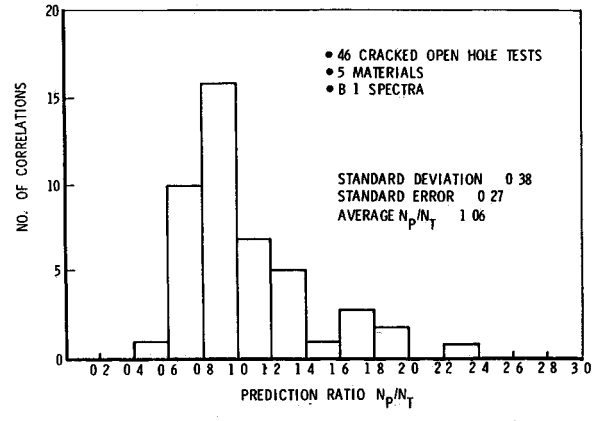

Fig 7 Histogram—CRKGRO predictions correlated with bomber spectrum test data

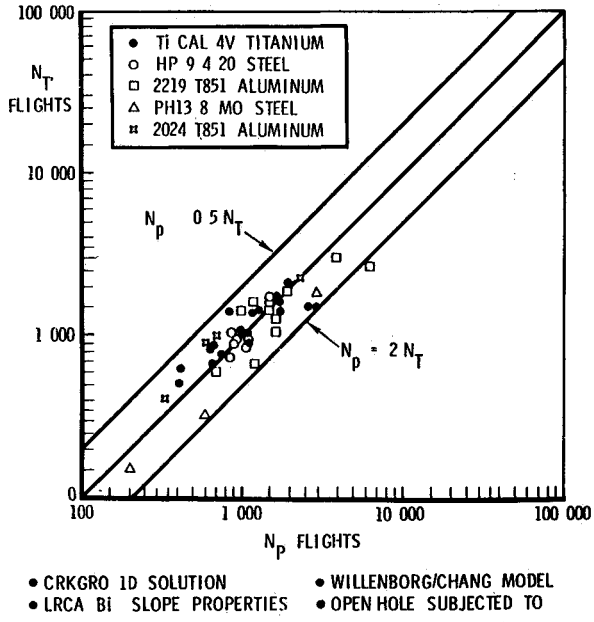

Fig 8 Correlation of predicted lift (N_P) to test life (N_T) for bomber spectrum

Table 2 Crack growth rate constants and material parameters

Material and product form	Environment	Upper slope				Lower slope				Transition point					
		C	n	m	q	C	n	m	q	ΔK, ksi $\sqrt{\text{in.}}$	da/dN, in./cycle	ΔK_{tho}[a] ksi $\sqrt{\text{in}}$	R_{cut}^{+}	R_{cut}	R_{so}[b]
Aluminum alloys															
2024-T81 sheet	Low-humidity air	3.499×10^{-10}	4.08	0.4	1.0	2.847×10^{-11}	5.89	0.4	1.0	7.0	2.7×10^{-6}	1.5	0.75	−0.50	2.3
2024-T851 plate	Low-humidity air	7.502×10^{-10}	3.92	0.6	1.0	1.826×10^{-11}	6.21	0.6	1.0	5.0	4.0×10^{-7}	1.5	0.75	−0.50	2.3
2124-T851 plate	Low-humidity air	1.373×10^{-9}	3.52	0.6	1.0	1.826×10^{-11}	6.21	0.6	1.0	5.0	4.0×10^{-7}	1.5	0.75	−0.50	2.3
	Sump tank water	1.516×10^{-9}	3.55	0.6	1.0	1.826×10^{-11}	6.21	0.6	1.0	5.0	4.0×10^{-7}	1.5	0.75	−0.50	2.3
	High-humidity air	1.240×10^{-9}	3.62	0.6	1.0	1.826×10^{-11}	6.21	0.6	1.0	5.0	4.0×10^{-7}	1.5	0.75	−0.50	2.3
2219-T851 plate	Low-humidity air	2.241×10^{-9}	3.22	0.6	1.0	2.126×10^{-13}	9.23	0.6	1.0	5.0	6.0×10^{-7}	1.5	0.75	−0.50	2.3
	Sump tank water	1.366×10^{-9}	3.54	0.6	1.0	2.126×10^{-13}	9.23	0.6	1.0	5.0	6.0×10^{-7}	1.5	0.75	−0.50	2.3
	High-humidity air	2.185×10^{-9}	3.27	0.6	1.0	2.126×10^{-13}	9.23	0.6	1.0	5.0	6.0×10^{-7}	1.5	0.75	−0.50	2.3
7075-T7351 and 7075-T7651 plate	Low-humidity air	1.035×10^{-9}	3.62	0.6	1.0	1.172×10^{-11}	6.53	0.6	1.0	5.5	8.0×10^{-7}	1.5	0.75	−0.50	2.65
	Sump tank water	2.626×10^{-9}	3.43	0.6	1.0	1.575×10^{-11}	6.56	0.6	1.0	6.0	2.0×10^{-6}	1.5	0.75	−0.50	2.65
7075-T73511 and 7075-T76511 extrusion	Low-humidity air	2.719×10^{-9}	3.73	0.6	1.0	1.514×10^{-11}	6.46	0.7	1.0	5.8	1.3×10^{-6}	1.5	0.75	−0.50	2.65
	Sump tank water	1.519×10^{-9}	3.94	0.6	1.0	1.832×10^{-11}	6.58	0.6	1.0	6.0	4.5×10^{-6}	1.5	0.75	−0.50	2.65
7175-T73652 hand forging	Low-humidity air	3.230×10^{-10}	4.17	0.6	1.0	5.99×10^{-14}	8.90	0.6	1.0	7.0	2.0×10^{-6}	1.5	0.75	−0.50	2.65
Steel alloys															
9Ni-4Co−0.20c (rolled plate and forged bar)	Low-humidity air	2.045×10^{-9}	2.50	0.7	1.0	1.183×10^{-12}	5.83	0.7	1.0	10.0	8.0×10^{-7}	5.5	0.75	−0.5	2.3
	High-humidity air	1.720×10^{-9}	2.61	0.7	1.0	1.183×10^{-12}	5.83	0.7	1.0	10.0	8.0×10^{-7}	5.5	0.75	−0.5	2.3
PH13-8Mo, cond H1000 (rolled bar)	Low-humidity air	3.59×10^{-10}	2.91	0.7	1.0	1.068×10^{-12}	5.21	0.7	1.0	14.0	1.0×10^{-6}	5.5	0.75	−0.5	3.5
	Sump tank water	4.313×10^{-12}	4.53	0.4	1.0	1.068×10^{-12}	5.21	0.7	1.0	14.0	1.0×10^{-6}	5.5	0.75	−0.5	3.5
PH13-8 Mo, cond H1000 (extruded bar)	Low-humidity air	4.057×10^{-10}	2.94	0.7	1.0	7.188×10^{-11}	3.72	0.7	1.0	13.0	1.0×10^{-6}	5.5	0.75	−0.5	3.5
300 M (forged bar)	Low-humidity air	1.001×10^{-9}	2.74	0.7	1.0	1.087×10^{-10}	3.81	0.7	1.0	10.0	7.0×10^{-7}	5.5	0.75	−0.5	3.5
AISI 9310 (rolled and forged bar)	Low-humidity air	3.502×10^{-10}	2.74	0.7	1.0	1.000×10^{-13}	6.64	0.7	1.0	8.0	1.0×10^{-7}	5.5	0.75	−0.5	3.5
	High-humidity air	1.098×10^{-9}	2.53	0.7	1.0	3.259×10^{-13}	6.41	0.7	1.0	8.0	2.0×10^{-7}	5.5	0.75	−0.5	3.5
9Ni-4Co.−0.30C (forged bar)	Low-humidity air	1.241×10^{-9}	2.64	0.7	1.0	2.452×10^{-12}	5.46	0.7	1.0	10.0	7.0×10^{-7}	5.5	0.75	−0.5	3.5
Titanium alloys															
Ti-6A1-4V plate (cond RA and cond DB	Low-humidity air	4.745×10^{-11}	3.89	0.6	1.0	1.43×10^{-13}	6.22	0.6	1.0	15.0	3.0×10^{-6}	4.5	0.60	−0.5	2.25
	Sump tank water	2.126×10^{-11}	4.21	0.4	1.0	5.779×10^{-14}	6.73	0.4	1.0	14.0	3.0×10^{-6}	4.5	0.60	−0.5	2.25
Ti-6A1-4V (hand forging, cond RA)	Low-humidity air	6.201×11^{-11}	3.70	0.4	1.0	9.508×10^{-14}	6.45	0.4	1.0	11.0	5.0×10^{-7}	4.5	0.60	−0.5	2.25
Nickel base alloy															
Inconel 718 (plate, bar,	Air at 70°F	2.840×10^{-11}	3.60	0.7	1.0	1.084×10^{-16}	8.35	0.7	1.0	14.0	4.0×10^{-7}	6.0	0.75	−0.5	3.5
	Air at 400°F	5.110×10^{-11}	3.60	0.7	1.0	1.950×10^{-16}	8.35	0.7	1.0	13.0	5.0×10^{-7}	5.0	0.75	−0.5	3.5

[a] $\Delta K_{th} = (1-AR)\,\Delta K_{tho}$, $A = 0$. [b] R_{SO} = overload shutoff ratio.

Table 3 Fighter baseline and spectrum variation tests, data correlations

Test No	Mission type	Test life N_T flt (cyc) $(C_i - C_f)$, in	CRKGRO Prediction Without load interaction N_P	N_P/N_T	Load interaction N_P	N_P/N_T
F B 1	A A baseline	2 829 (73 552) (0.145 to failure)	1 573 (41 189)	0 56	2,153 (55 164)	0 75
F B 2	A G baseline	5 403 (102 677) (0,148 to failure)	3,084 (74 954)	0 73	4,949 (94 463)	0 92
F B-3	I N baseline	30 142 (162,721) (0 145 to failure)	19 595 (109 019)	0 65	28 584 (159 335)	0 95
F B 4	Composite baseline	5 174 (106 705) (0 148 to failure)	2,490 (51 218)	0 48	3 317 (68 291)	0.64
FB V A 1	A A zero comp	3 405 (88 528) (0 145 to failure)	1,573 (40 723)	0 46	3,021 (78,790)	0 89
FB V A 2	A G zero comp	5,429 (103,161) (0 15 to failure)	3 796 (72 213)	0 70	5 826 (110 382)	1 07
FB V A 3	I N zero comp	34,720 (193,202) (0 145 to failure)	19 944 (110 125)	0 57	34 955 (195 134)	1 01
FB V A 4	Composite zero comp	5 995 (123,689) (0 145 to failure)	2 491 (51 949)	0 42	4 965 (102,662)	0 83
FB V-B-3	I N DLS = 25 ksi	40,080 (222.331) (0 145 to 0 83)	36 875 (204 544)	0 92	54 186 (300 147)	1 35
FB V B 4	Composite DLS = 25 ksi	7 736 (159,514) (0 145 to 0 61)	4 302 (89 328)	0 56	5 909 (121 231)	0 76
FB V C 1	A A DLS = 35 ksi	1 293 (33 616) (0 145 to failure)	,878 (22 859)	0 68	1 101 (28 574)	0 85
FB V C 2	A G DLS = 35 ksi	2 867 (55 045) (0 145 to failure)	2 176 (41 284	0 75	2 706 (51 192)	0 93
FB V C 3	I-N DLS = 35 ksi	19 073 (106,164) (0 145 to failure)	10 955 (60 513)	0 57	16 000 (89 178)	0 84
FB V C 4	Composite DLS = 35 ksi	2 303 (47 683) (0 145 to failure)	1 273 (26,226)	0 55	1 855 (38 146)	0.80
FB V D 1	A A 85% DLS clipping	1 939 (50 414) (0 145 to failure)	1,653 (42 852)	0 85	1 922 (49 910)	0 99
FB V D 4	Composite 85% DLS clipping	2 924 (60 480) (0 145 to failure)	2,516 (52 013)	0 86	3,134 (64 714)	1 07
FB V E 1	A A 95% DLS clipping	2 133 (55 467) (0 145 to failure)	1,618 (42 069)	0 76	1,990 (51 739)	0 93
FB V E 4	Composite 95% DLS clipping	3,847 (79 490) (0 145 to failure)	2 493 (51 506)	0:65	3 298 (67 979)	0 86

Table 3 Continued

Test No	Mission type	Test life N_T flt (cyc) $(C_i - C_f)$, in	CRKGRO Prediction Without load interaction N_P	N_P/N_T	Load interaction N_P	N_P/N_T
FB V F 4	Composite 35% DLS truncation	4 864 (75 723) (0 145 to failure)	2 493 (38 619)	0 51	3 137 (51 492)	0 68
FB V G 4	Composite 45% DLS truncation	5 171 (52 293) (0 148 to failure)	2 905 (29 284)	0 56	3 729 (37 651)	0 72
FB V-H 4	Composite 55% DLS truncation	6 833 (35 414) (0 145 to failure)	3 953 (20 540)	0 58	5,171 (26 915)	0 76
FB V I 4	Composite mission sequence (A)	4 965 (102 459) (0 145 to failure)	2 491 (51 445)	0 50	3,333 (68 911)	0 67
FB V J 4	Composite mission sequence (B)	4 392 (90 576) (0 145 to failure)	2 518 (51 849)	0 57	3,362 (69 344)	0 77
FB V K 4	Composite comp load increased 25%	4 775 (98 635) (0 145 to failure)	2 491 (51,445)	0 52	3 111 (64 243)	0 65
FB V L 4	Composite comp load increased 50%	4 347 (89,721) (0 145 to failure	2,491 (51 445)	0 57	2 905 (59 997)	0 67
M 301	Mission mix variation A-1	3 895 (68 833) (0 135 to failure)	3 580	0 92	4 765	1 22
M 302	Mission mix variation A 2	4,127 (71 925) (0 145 to failure)	3 459	0 84	4 417	1 07
M 303	Mission mix variation A 3	5,258 (79 574) (0 145 to failure)	4 348	0 83	5 941	1 13
M 304	Mission mix variation A 4	4 839 (75 084) (0 150 to failure)	3 664	0 76	5 107	1 05
M 305	Mission mix variation A 5	4 390 (75 641) (0 150 to failure)	3 131	0 71	4 178	0 95
M 306	Mission mix variation B 1	5 667 (96 867) (0 145 to failure)	3 111 (53 354)	0 55	4,843 (82 785)	0 85
M 307	Mission mix variation B 2	5,583 (92 031) (0 148 to failure)	2 905 (47,985)	0 52	3 935 (64,925)	0 71
M-308	Mission mix variation B 3	13 296 (186,390) (0 148 to failure)	4,641 (65 087)	0 35	9 382 (131 556)	0 71
Average prediction ratio				0 64		0 88
Standard deviation				0 15		0 17

solutions were obtained without accounting for the tensile overload retardation effect Furthermore all compressive load cycles were clipped to zero

To assess prediction accuracy, the ratio of predicted crack growth life to test life, N_p/N_t, was calculated for each of the 33 test cases Table 3 summarizes the results A histogram for the fighter spectrum test case correlations is shown in Fig 5 The average prediction ratio is $(N_p/N_t)=0\ 88$ with a 0 17 standard deviation for "load interaction"[14] solutions The average (N_p/N_t) for "without load interaction" solutions was 0.64 with a 0 15 standard deviation Results indicated that the load interaction model predicted the fatigue crack growth lives more accurately than the without load interaction counterparts It can be seen from Fig 5 that the majority (78%) of the predictions which accounted for load-interaction effects correlated with test data were $[0.7 \le (N_p/N_T) \le 1\ 3]$ To further illustrate this point, a plot of predicted lives obtained from the load interaction option of CRKGRO vs the test lives for the 33 test cases was made as shown in Fig 6 It can be seen that most of the points were bounded between $N_p = 1\ 5\ N_t$ and $N_p = 0\ 75\ N_t$ lines

Bomber Spectra Test Data Correlations

A total of 46 sets of test data of corner cracks emanating at open holes contained in panels subjected to various types of bomber spectra[24] were correlated Specimens used in this test group were fabricated from five materials: 2219 T851 and 2024 T851 aluminum alloys; HP9 4 20 and PH13 8 steel alloys; as well as Ti 6Al 4V titanium alloy.

The test spectra in this test group were the wing and wing carry-through structure spectrum, fuselage spectrum, and the empennage spectrum of a bomber class aircraft All spectra were composite missions in the flight by-flight format with infrequent peak load cycles which occur either every tenth flight or in every one hundredth flight All tests were con ducted similarly to the fighter spectrum tests Except in a few cases, tests were conducted in sump tank water (STW) en vironment

All predictions were performed by the load interaction option of CRKGRO only The crack growth rate constants and load interaction model parameters employed in the correlations for the previously mentioned materials are listed in Table 2 All analytical predictions were done by CRKGRO's 1 D analysis option This is because all the cracks were initially in the nearly stable shape (i e , the aspect ratio of the crack is approximately $a/2c = 0\ 5$) Again, the prediction ratio was calculated for each of the 46 test cases The histogram shown in Fig 7 indicates the distribution of the prediction ratios The average prediction ratio was $(N_p/N_t)_{ave} = 1\ 06$ with a 0 27 standard error, which demonstrated the predictability of the methodology. To study the material variance, a plot of predicted lives vs test lives for each material was constructed as shown in Fig 8 It can be seen that the prediction accuracies were independent of materials

Transport Spectrum Test Data Correlations

The test data correlated in this category were generated from the research work documented in Ref 16 The flight spectra used in the test program were derived from an ad vanced military transport baseline composite mission which consisted of three basic missions: assault (A) logistics (L), and training (T) Each mission was composed of four segments: climb cruise, gust, and descent A uniblock of 21 flights was derived and used in the test In addition to the baseline composite spectrum test, seven more transport spectrum variation tests were conducted, which included the following:

1) Tension and compression stresses were increased by 60%

2) Compressive stresses were set to zero

3) Compressive stresses were increased by 25%

4) Compressive stresses were increased by 50%

5) Cycles with maximum stresses less than 8 ksi were truncated

6) The minimum stresses of those cycles with stress ratio (R) greater than 0 75 were lowered to $\sigma_{min} = 0\ 75\ \sigma_{max}$

7) All cycles were deleted except the ground-air-ground (G A G) in a flight

Test specimens were CCT specimens machined from the same heat of 2219 T851 aluminum plates used in the previously described fighter spectrum test program All tests

Table 4 Comparison of prediction accuracy for transport spectra cases—with or without considering load interaction effects

Test No	Mission type	Test life N_T flt (cyc) $(C_i - C_f)$, in	CRKGRO prediction: Load interaction N_P	N_P/N_T	Without load interaction N_P	N_P/N_T
T B 1	Composite baseline	9 675 (1 284 857) 0 26 0 505	9 421 (1 251 109)	0 97	16 110 (2,139 375)	1 67
T B V-1	Zero out compression	10 972 (1,457,138) 0 255 0 48	19 239 (2 555 089)	1 75	16 476 (2 188 212)	1 50
T B V 2	Increasing stress level by 1 6 factor	2 751 (365,314) 0 26 0 568	1 730 (229 792)	0 63	2 952 (392,086)	1 07
T B V 4	Increasing comp load by 50%	7 364 (997,990) 0 258 0 44	8 086 (1 073 380)	1 10	13 844 (1 838 498)	1 88
T B V 5	Increasing comp load by 25%	8 013 (1 064 251) 0 255 0.458	8 766 (1 164 107)	1 09	15 003 (1 992 440	1 87
T B V 7	Truncating low load cycles below 8 ksi	9 969 0 265 0 493	9 316 (1 060 169)	0 93	15 921	1 60
T B V 8	Lowering min stress to 0 75 σ_{max}	4 317 (573 280) 0 255 0 488	5 360 (711 838)	1 24	6,481 (960 690)	1 50
T B V 9	G A G cycles only	16 535 (16 535) 0 26 0 505	11 648 (11 648)	0 70	27 357 (27 357)	1 65
Average prediction ratio				1 05		1 59
Standard deviation				0 35		0 26

were run in laboratory air at room temperature The cyclic rate was approximately 5 Hz Due to the relative low stress level, the fatigue crack growth lives of these specimens were anticipated to be very long Hence, each test was terminated before the crack reached its critical size

Analytical predictions were performed again by using the CRKGRO program Material data inputs were identical to those used in the fighter spectrum data correlation cases. Both the load interaction solutions and the without load interaction solutions were obtained Results of the analytical predictions for these eight transport spectrum test cases are summarized in Table 4, together with the test results As shown in the table, for the load interaction solutions, the average prediction ratio for these eight cases was $(N_p/N_t)_{ave} = 1\ 05$ with an 0 29 standard error For the without load interaction solutions, $(N_p/N_t)_{ave} = 1\ 59$ with an 0.6 standard error Note that the load interaction solutions were much more accurate than their without load interaction counterparts The fact that predicted lives, which accounted for load interaction effects, were shorter than those without accounting for load-interaction effects demonstrated the big influence of compressive loads to the crack growth in this type of spectrum. This is because the G A G cycle of each flight contributed 60% of the damage Consequently, overestimation of lives resulted if the compressive portion of the G-A G cycles were neglected

Concluding Remarks

An improved damage tolerance analysis methodology for predicting the fatigue crack growth of a crack or a cracklike flaw contained in metallic airframe structures subjected to random cycle-by-cycle spectrum loadings is presented This improved analytical methodology has been demonstrated to be able to provide accurate predictions for various classes of aircraft and various families of metallic materials The ap plication of this improved methodology will not be limited to only aircraft structures It can be employed to perform fatigue crack growth analyses on spacecrafts, offshore oil drilling platforms, high transmission steel towers and many other structures that are subjected to spectrum loadings

Acknowledgment

This program is based on part of the results of a development task performed on Contract F33615 77 C 3121, sponsored by the Air Force Wright Aeronautical Laboratory, Wright-Patterson Air Force Base Ohio

References

[1] ' Military Standard Aircraft Structural Integrity Program Airplane Requirements, MIL STD-1530A Dec 1975

[2] Military Specification, Airplane Damage Tolerance Requirements, ' MIL A-83444A, July 1974

[3] ' Federal Aviation Regulation Airworthiness Standard Tran sport Category Airplane,' FAR 25 571, Amendment 45.

[4] Engle R M , CRACKS, A Fortran IV Digital Computer Program for Crack Propagation Analysis AFFDL TR 70 107, Air Force Flight Dynamics Laboratory Wright-Patterson AFB Ohio 1970

[5] Szamossi, M Crack Propagation Analysis by Vroman s Model, Program EFFGRO NA 72 94 Rockwell International B 1 Division, Los Angeles Calif 1972

[6] Kan H P , Reed H L and Liu A F , ' Crack Propagation Predictive Analysis Computer Program FLAGRO User s Manual, STR-310 Space Division Rockwell International Downey Calif 1976

[7] Johnson W S and Spamar, T , A User s Guide to CGR GD, A Computerized Crack Growth Predicting Program General Dynamics Report FZ5 241 1976

[8] Newman J. C , A Crack Closure Model for Predicting Fatigue Crack Growth Under Aircraft Spectrum Loading ASTM STP 748 American Society for Testing and Materials 1981

[9] Engle, R M., Aspect Ratio Variability in Part Through Crack Life Analysis, ASTM STP 687 American Society for Testing and Materials 1979

[10] Chang J B ' Improved Methods for Predicting Spectrum Loading Effects, Fifth Quarterly Report NA 78 491 5, North American Aircraft Div Rockwell International Los Angeles Calif 1979.

[11] Chang J B , Szamossi, M and Liu, K W Random Spectrum Fatigue Crack Life Predictions with or Without Considering Load Interactions, ' ASTM STP 748 American Society for Testing and Materials, 1981

[12] Rudd J L and Engle, R M 'Crack Growth Behavior of Center Cracked Panels under Random Spectrum Loading ASTM STP 748 American Society for Testing and Materials 1981

[13] Chang, J B Engle, R M and Szamossi M An Improved Methodology for Predicting Random Spectrum Load Interaction Effects on Fatigue Crack Growth ' *Proceedings of Fifth International Conference on Fracture* Pergamon Press New York 1981

[14] Romanelli M J , Runge Kutta Method for the Solution of Ordinary Differential Equation ' *Mathematical Methods for Digital Computers* John Wiley and Sons, New York, 1960

[15] Chang, J B Szamossi M and Liu K W A User s Manual for a Detailed Level Fatigue Crack Growth Analysis Computer Code Volume I: The CRKGRO Program AFWAL TR 81 3093 Vol I Air Force Wright Aeronautical Laboratories Wright Patterson AFB Ohio, 1981

[16] Chang, J B Hiyama, R M and Szamossi M Improved Methods for Predicting Spectrum Loading Effects, Vol I Technical Summary,' AFWAL TR 81 3092 Vol. I Air Force Wright Aeronautical Laboratories Wright Patterson AFB, Ohio 1981

[17] Walker, K , The Effect of Stress Ratio During Crack Propagation and Fatigue for 2024 T3 and 7075 T6 Aluminum ' ASTM STP 462 American Society for Testing and Materials, 1970

[18] Gallagher, J P , A Generalized Development of Yield Zone Models ' AFFDL TM 74 28 Air Force Flight Dynamics Laboratory Wright-Patterson AFB Ohio, 1974.

[19] Newman J C Jr and Raju I S 'Analysis or Surface Crack in a Finite Plate Under Tension or Bending Loads " NASA TP 1578 NASA Langley Research Center Hampton Va 1979

[20] Hartranft, R J and Sih, G C , An Approximate Three Dimensional Theory of Plate With Application to Crack Problems *International Journal of Engineering Science* Vol 8 No 8 1970

[21] Streittmatter, S , A Method of Counting Spectrum Load Cycles ' TFD 72 358 B 1 Division Rockwell International Los Angles, Calif , 1972

[22] Schijve, J , Analysis of Random Load Time Histories With Relation to Fatigue Tests and Life Calculations *Fatigue of Aircraft Structures* Pergamon Press New York 1963

[23] Chang, J B Engle R M , and Szamossi, M , Numerical Techniques in Computer Aided Fatigue Crack Growth Analysis *Proceedings of the Second International Conference on Numerical Methods in Fracture Mechanics* Pineridge Press Sevansea United Kingdom 1980

[24] Stolpestad, J H Summary Report of the Fracture Mechanics Analysis Verification Test Program, NA 75 675 Rockwell In ternational Los Angeles Calif 1975